Received: 2 May 2021 | Revised: 2 September 2021 | Accepted: 10 September 2021

IET Power Electronics

DOI: 10.1049/pel2.12196

The Institution of Engineering and Technology WILEY

ORIGINAL RESEARCH PAPER

Design, analysis and implementation of a new three-port DC-DC converter with bidirectional capability

Tohid Jalilzadeh[1] | **Naghi Rostami**[1] | **Ebrahim Babaei**[1,2] | **Seyed Hossein Hosseini**[1,2]

[1] Faculty of Electrical and Computer Engineering, University of Tabriz, 29 Bahman Blvd., Tabriz, Iran

[2] Engineering Faculty, Near East University, North Cyprus, Mersin 10, Nicosia 99138, Turkey

Correspondence
Naghi Rostami, Faculty of Electrical and Computer Engineering, University of Tabriz, Tabriz 51666-16471, Iran.
Email: n-rostami@tabrizu.ac.ir

Funding information
Iran National Science Foundation (INSF), Grant/Award Number: 98001298

Abstract

The proposed converter here is a dual-input DC-DC converter with bidirectional power flow. One of the inputs is unidirectional, while the other is a bidirectional port for a battery. The proposed converter can combine two alternating sources with different characteristics. The demanded power of the load can be provided by each input source individually or simultaneously. What is more, the unidirectional port can charge the battery as well as power the output load. Due to the bidirectional capability, the energy returned from the output can be stored in the battery which is suitable for electric vehicle (EV) applications. Step-up capability, the low voltage stress on semiconductors, and the smaller number of passive elements are the other advantages of the converter. Depending on the battery usage status, four different operation scenarios are defined in the proposed converter. The converter operation is described in each scenario and the mathematical analysis is presented. Based on these, the experimental prototype is conducted to verify the characteristics and feasibilities of the converter.

1 | INTRODUCTION

Renewable sources are increasingly used due to environmental concerns and technological advances [1–4]. However, the intermittent nature of these sources and the unpredictability of load demand poses a challenge to the widespread development of these energy sources [5, 6]. Therefore, due to the inherent change in the terminal voltage of these sources, the use of voltage converters between the source and the load/grid to control the output voltage is inevitable [7]. On the other hand, the output voltages of these sources are so low that they are not suitable for many applications. To increase the DC voltage values, DC-DC converter interfaces must be used [8]. The dependence of some renewable energy sources on the climate has led to a tendency to combine different types of sources to provide power with high quality and reliability for load feeding [9]. To meet load demand and solve the challenge of the alternative nature of renewable energy and the unpredictability of load demand, usually power electronic converters are integrated with energy storage systems. The multi-input (MI) converter is a solution to meet the requirements of some applications that require the integration of several types of input energy sources [10].

Reference [11] presents a bidirectional MI structure that can operate independently in three modes of buck, boost, or buck-boost. The need to use a high-inductance inductor which leads to an increase in the size and weight of the converter, as well as its inability to simultaneously transfer the energy of input sources to the output are the drawbacks of the converter. The converter in [12] can operate in buck and boost modes with bidirectional power control. The need to use an independent inductor for each input source increases the volume and weight of the converter for a large number of inputs. Two step-up unidirectional three-input DC-DC converters are provided in [13, 14], which have two unidirectional input ports and one bidirectional port. The excessive number of current path switches, higher losses, and inability to operate in the buck or buck-boost modes are the main disadvantages of the structures. An MI converter with bidirectional power flow is provided in [15] which can operate in buck and buck-boost modes. This structure requires a separate inductor for each input source, which increases in size and cost. The MI converter with step-up capability is presented in [16]. To increase the voltage gain, the number of input sources is increased, which increases the number of components and in turn, the size, volume and weight of

the converter. The impossibility of the converter to operating as bidirectional is another drawback. A switched-capacitor-diode-based MI converter with high voltage gain is presented in [17] which utilizes a higher number of components. The lack of common ground between the input and output ports is another disadvantage of the converter. A non-isolated step-up MI converter utilizing coupled-inductor and clamp circuit is presented in [18] in which there is no common ground between input and output ports. Besides, this converter cannot operate as a bidirectional converter. A quadratic-based three-port converter with a simultaneous power transfer of the input ports is presented in [19] in which the battery port does not share common ground with other input and output ports. On the other hand, the power flow is not bidirectional. A high-voltage gain dual-input DC-DC converter with bidirectional power flow is presented in [20]. The impossibility of simultaneous power transfer of input sources and the high voltage stress of the switches are the major drawbacks of this converter. The converter in [21] is another MI converter with high step-up and soft-switching capabilities in which the bidirectional power flow is not provided. A three-port bidirectional DC-DC converter presented in [22] integrates a PV panel and a battery in a DC nanogrid. The most important disadvantage of this converter is the lack of common ground between the ports. Another coupled-inductor-based three-port DC-DC converter with bidirectional power flow is presented in [23]. In [24], a dual-input DC-DC converter is presented in which the power flow is not bidirectional. Another drawback of this converter is its inability to simultaneous power transfer of the input sources. The couple-inductor-based three-port DC-DC converter in [25] has high voltage gain, however, the power flow direction is unidirectional. Furthermore, the two inputs have no common grounding. Another dual-input DC-DC converter with a high number of diodes is introduced in [26]. In this converter, the bidirectional power flow is not provided and the voltage stress across the semiconductors is high. Reference [27] presents a bidirectional DC-DC converter in which there are no common grounds between the ports. Besides, charging of the battery is not provided via another input or from the output energy. The high voltage stress on the semiconductors is another drawback of this structure. A high-voltage-gain DC-DC converter with dual input and unidirectional power flow is investigated in [28] in which the input ports do not share the common ground. The high number of diodes and capacitors is another disadvantage of the converter.

The novelty of the proposed converter is summarized as follows:

1. Bidirectional power flow capability by operating the converter in buck mode.
2. Simultaneous and individual power transfer from the input sources to the output load which states the flexibility of the converter.
3. Battery charging by another input source (V_1) and the energy returned from the output, preventing the battery from complete-depleting and the energy from wasting.
4. Common grounding between the input and output ports. This feature causes the converter to have high safety and fewer protection problems and electromagnetic interference. Besides, there is no addition dv/dt between input and output grounds.
5. Voltage step-up capability which allows the proposed converter to be used in renewable energy applications, with one input being a battery and the other input being a photovoltaic panel (PV) or fuel cell (FC).
6. Reduced peak voltage stress (PVS) of the semiconductor devices. Lower PVS results in utilizing power switches with small ON-state resistance and the diodes with lower nominal voltage which reduces the conduction and turn-on losses and improves the efficiency.
7. Improved dynamic performance due to the lower number of passive devices (inductors and capacitors). Good dynamic performance allows the proposed converter to respond more quickly to changes in input voltage, output load, or duty cycles, and the range of change is negligible.

Based on the above-mentioned advantages, the proposed converter can be a good candidate for electric vehicle (EV) applications where the energy-returning from the output should charge the battery. Furthermore, the proposed converter can be applicable in renewable energy systems in which different energy sources with different characteristics such as PV or FC can connect to a unidirectional input port, and the other port is the battery.

The paper is organized as follows: Section 2 is dedicated to the operation principles of the converter. In Section 3 the dynamic modelling is investigated. The control method and design procedure are given in Sections 4 and 5, respectively. An investigation of the semiconductors' voltage and current stresses is done in Section 6. A comparison of the converter with other solutions is carried out in Section 7. Analysis of the loss and thermal distribution is done in Section 8. The experimental results of the laboratory prototype are presented in Section 9 and the last section concludes the paper.

2 | OPERATION MODES OF THE PROPOSED CONVERTER

The power circuit of the proposed converter is shown in Figure 1 In this converter, V_1 is a unidirectional port and V_b is a bidirectional port. With proper switching of switches S_1-S_5, T_1, and T_2, output voltage and battery charge/discharge current can be regulated.

Two power diodes (D_1, D_2), two inductors (L_1, L_2), and a capacitor (C_o) are also used in the proposed converter. D_1 prevents current from returning to port V_1. Besides, D_2 is used in the phase energy returning from the output which creates a path for L_2 current. In cases where the input source is PV, the current ripple of the input source must be minimized to create an accurate power balance between powers the input and the output load. So, the CCM operation is analysed.

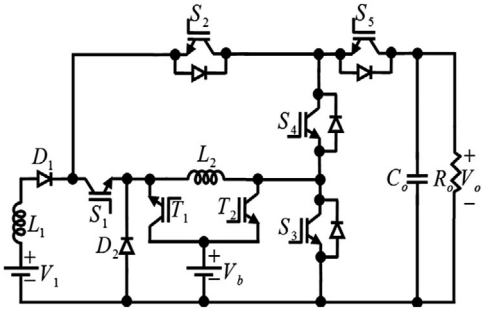

FIGURE 1 Power circuit of the proposed DC-DC converter

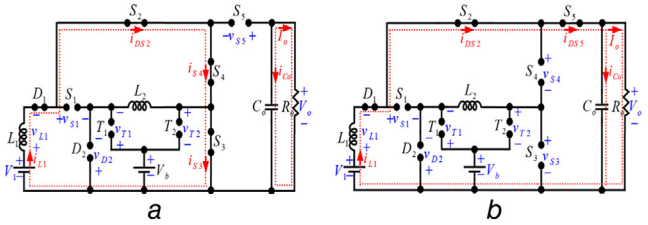

FIGURE 2 Equivalent circuits in the first scenario; (a) subinterval I, (b) subinterval II

2.1 | Unidirectional power flow operation

In unidirectional operation, the power transfer direction is from input sources to the output load (R_o). Depending on the different switching schemes, different operation scenarios are obtained, which are discussed in detail below:

2.1.1 | First scenario (The load is powered by V_1)

In this scenario, R_o is supplied only by V_1, and the battery is not used. During this scenario, S_1 is permanently OFF, and therefore, L_2 is not used. In a switching period (T) there are two switching subintervals as shown in Figure 2a b. These two subintervals are examined in detail below:

Switching subinterval I ($0 < t < d_{S4}T$): According to Figure 2a in this subinterval, S_3 and S_4 are ON and S_5 is OFF. Besides, the body diode of S_2 is directly biased, creating a path for i_{L1}. The voltage and current equations of L_1 and C_o are as follows in which r_1 represents the ESR of L_1:

$$L_1\dot{i}_{L1} = V_1 - r_1 i_{L1} \tag{1}$$

$$C_o\dot{V}_o = -I_o \tag{2}$$

Switching subinterval II ($d_{S4}T < t < T$): At $t = d_{S4}T$, S_3 and S_4 are turned off simultaneously, while due to the energy stored in L_1, the body diode of S_2 remains forward biased.

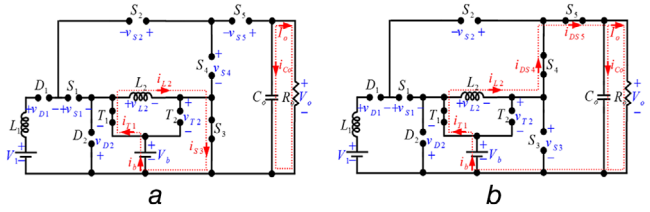

FIGURE 3 Equivalent circuits in the second scenario; (a) subinterval I, (b) subinterval II

Besides, the body diode of S_5 conducts to deliver the energy of L_1 to R_o. Based on Figure 2b these equations are written:

$$L_1\dot{i}_{L1} = V_1 - V_o - r_1 i_{L1} \tag{3}$$

$$C_o\dot{V}_o = i_{L1} - I_o \tag{4}$$

By applying the volt-second and current-second balance laws to L_1 and C_o, the following equations are obtained:

$$V_o = \frac{V_1 - r_1 i_{L1}}{1 - d_{S4}} \tag{5}$$

$$(1 - d_{S4})i_{L1} = I_o \tag{6}$$

2.1.2 | Second scenario (The load is powered by V_b)

There are cases where the load should be supplied only through the battery. For example, if V_1 is the PV output voltage, PV cannot supply the load at night. In such cases, the battery is responsible for feeding the load. In this scenario, T_1 is always ON and V_o can be controlled by properly controlling S_3. This scenario is divided into two subintervals as shown in Figure 3 and is analysed below:

Switching subinterval I ($0 < t < d_{S3}T$): In this subinterval, T_1 and S_3 are turned on while the other switches are OFF. So, i_b increases linearly and leads to battery discharge. These equations are written from Figure 3a

$$L_2\dot{i}_{L2} = V_b - r_2 i_{L2} \tag{7}$$

$$C_o\dot{V}_o = -I_o \tag{8}$$

Switching subinterval II ($d_{S3}T < t < T$): As shown in Figure 3b T_1 is still ON while S_3 is OFF in this subinterval. So, the body diode of S_4 and S_5 is directly biased to create a path for i_{L2}. The following equations can be obtained:

$$L_2\dot{i}_{L2} = V_b - V_o - r_2 i_{L2} \tag{9}$$

$$C_o\dot{V}_o = i_{L2} - I_o \tag{10}$$

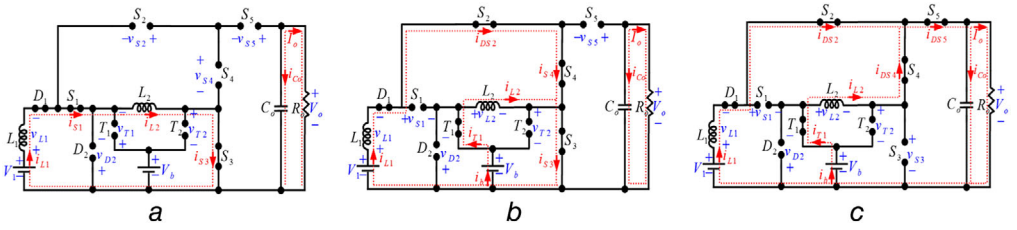

FIGURE 4 Equivalent circuits in the third scenario; (a) subinterval I, (b) subinterval II, (c) subinterval III

By applying the volt-second and current-second balance laws to L_2 and C_o, the following equations are obtained:

$$V_o = \frac{V_b - r_2 i_{L2}}{1 - d_{S3}} \tag{11}$$

$$(1 - d_{S3}) i_{L2} = I_o \tag{12}$$

In this operating scenario, battery current and power are determined as follows:

$$i_b = i_{L2} \tag{13}$$

$$P_b = V_b i_{L2} \tag{14}$$

2.1.3 | Third scenario (The load is powered by V_1 and V_b)

In this scenario, the load is supplied by V_1 and the battery. Therefore, in this scenario, battery discharge occurs. By controlling S_3, the battery discharge power can be adjusted. Figure 4a c shows the equivalent circuits of the proposed converter during this scenario.

Switching subinterval I ($0 < t < d_{S1} T$): In this subinterval, L_1 and L_2 are magnetized through V_1 and the battery is not used. Therefore, S_1 and S_3 are ON and the other switches are OFF. From Figure 4a the following equations are obtained:

$$(L_1 + L_2)\dot{i}_{L1} = V_1 - (r_1 + r_2) i_{L1} \tag{15}$$

$$C_o \dot{V}_o = -I_o \tag{16}$$

Switching subinterval II ($d_{S1} T < t < d_{S3} T$): At $t_1 = d_{S1} T$, S_1 is turned off and T_1 and S_4 are turned on. S_3 is still ON, and the body diode of S_2 is directly biased to conduct i_{L1}. The following equations can be written according to Figure 4b

$$L_1 \dot{i}_{L1} = V_1 - r_1 i_{L1} \tag{17}$$

$$L_2 \dot{i}_{L2} = V_b - r_2 i_{L2} \tag{18}$$

$$C_o \dot{V}_o = -I_o \tag{19}$$

Switching subinterval III ($d_{S3} T < t < T$): In this subinterval, the energy of L_1 and L_2 is transferred to the output. Therefore, S_3 and S_4 are turned off and the body diode of S_4 conducts. As shown in Figure 4c the following equations are obtained for the voltage and current of L_1, L_2, and C_o:

$$L_1 \dot{i}_{L1} = V_1 - V_o - r_1 i_{L1} \tag{20}$$

$$L_2 \dot{i}_{L2} = V_b - V_o - r_2 i_{L2} \tag{21}$$

$$C_o \dot{V}_o = i_{L1} + i_{L2} - I_o \tag{22}$$

Applying volt-second and current-second balance laws to L_1, L_2, C_o and using $d_{T1} = 1\text{-}d_{S1}$ results in the following equations:

$$V_o = \frac{V_1 + d_{T1} V_b - r_1 i_{L1} - r_2 i_{L2}}{2(1 - d_{S3})} \tag{23}$$

$$(1 - d_{S3})(i_{L1} + i_{L2}) = I_o \tag{24}$$

In this scenario, the load is supplied from V_1 and the battery. Therefore, the current and power taken from the battery are calculated as Equations (25) and (26):

$$i_b = d_{T1} i_{L2} \tag{25}$$

$$P_b = V_b d_{T1} i_{L2} \tag{26}$$

2.1.4 | Forth scenario (V_1 powers the load and charges the battery)

In this scenario, V_1 not only supplies the load but also charges the battery. Therefore, d_{T2} can be controlled to adjust the charge current/power of the battery. V_o control can be done by controlling d_{S3}. It is noteworthy that in this scenario, S_1 is always ON. Figure 5a -c shows the equivalent circuits in this scenario.

Switching subinterval I ($0 < t < d_{S3} T$): In this subinterval, L_1 and L_2 are magnetized in series by V_1. Therefore, all switches except S_1 and S_3 are OFF. The following equations can be

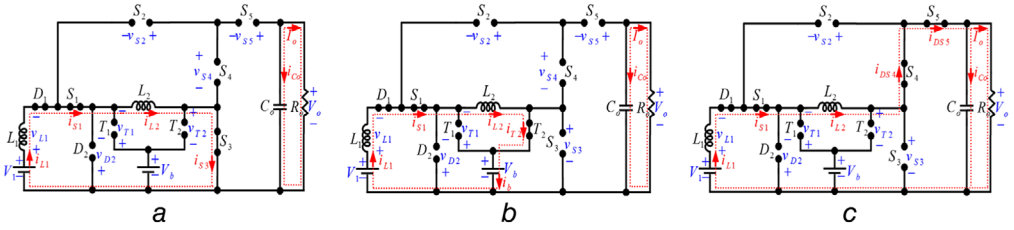

FIGURE 5 Equivalent circuits in the fourth scenario; (a) subinterval I, (b) subinterval II, (c) subinterval III

written according to Figure 5a

$$(L_1 + L_2)\dot{i}_{L1} = (L_1 + L_2)\dot{i}_{L2} = V_1 - (r_1 + r_2)i_{L1} \quad (27)$$

$$C_o\dot{V}_o = -I_o \quad (28)$$

Switching subinterval II ($d_{S3}T < t < (d_{T2}+d_{S3})T$): At $t_1 = d_{S3}T$, S_3 is turned off and T_2 is turned on. In this subinterval, L_1 and L_2 have magnetized again and the process of charging the battery is performed. Figure 5b shows that:

$$(L_1 + L_2)\dot{i}_{L1} = (L_1 + L_2)\dot{i}_{L2} = V_1 - V_b - (r_1 + r_2)i_{L1} \quad (29)$$

$$C_o\dot{V}_o = -I_o \quad (30)$$

Switching subinterval III ($(d_{T2}+d_{S3})T < t < T$): The energy stored in L_1 and L_2 in the previous subintervals in this subinterval is transferred to the load. For this reason, the body diode of S_4 conducts. From Figure 5c the following equations are written:

$$(L_1 + L_2)\dot{i}_{L1} = (L_1 + L_2)\dot{i}_{L2} = V_1 - V_o - (r_1 + r_2)i_{L1} \quad (31)$$

$$C_o\dot{V}_o = i_{L1} - I_o = i_{L2} - I_o \quad (32)$$

According to the volt-second and current-second balance laws, the following equations are obtained:

$$V_o = \frac{V_1 - d_{T2}V_b - (r_1 + r_2)i_{L1}}{1 - d_{T2} - d_{S3}} \quad (33)$$

$$(1 - d_{T2} - d_{S3})i_{L1} = (1 - d_{T2} - d_{S3})i_{L2} = I_o \quad (34)$$

In this scenario, load power is supplied from V_1. Besides, V_1 is responsible for charging the battery. Therefore, the current and power delivered to the battery are calculated as relations in Equations (35) and (36):

$$i_b = d_{T2}i_{L1} \quad (35)$$

$$P_b = -V_b d_{T2} i_{L1} \quad (36)$$

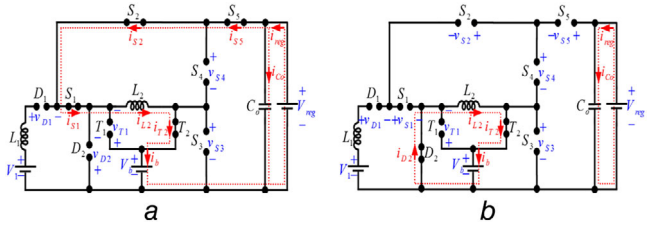

FIGURE 6 Equivalent circuits in bidirectional power flow operation; (a) subinterval I, (b) subinterval II

2.2 | Bidirectional power flow operation

In this operation mode, the energy returned from the output is stored in the battery. So, T_2 is always ON. To test the bidirectional capability of the proposed converter, the voltage source V_{reg} is placed in the output port and by switching S_1, S_2, and S_5, the energy is transferred to the battery. Figure 6a b shows the subintervals in this mode.

Switching subinterval I ($0 < t < d_{S5}T$): As shown in Figure 6a S_5 is ON in this subinterval to transfer the output energy to the battery. Besides, S_1, S_2, and T_2 are ON, and D_1 is reverse biased. Thus, L_2 is magnetized. The following equations are obtained:

$$L_2\dot{i}_{L2} = V_{reg} - V_b - r_2 i_{L2} \quad (37)$$

$$C_o\dot{V}_{reg} = i_{reg} - i_{L2} \quad (38)$$

Switching subinterval II ($d_{S5}T < t < T$): At $t_1 = d_{S5}T$, S_1, S_2, and S_5 are turned off while T_2 is still ON. Besides, D_2 is directly biased, creating a freewheeling path for i_{L2}. It is clear from Figure 6b that:

$$L_2\dot{i}_{L2} = -V_b - r_2 i_{L2} \quad (39)$$

$$C_o\dot{V}_{reg} = i_{reg} \quad (40)$$

Applying volt-second and current-second balance laws to L_2 and C_o result in the following equations:

$$V_b = d_{S5}V_{reg} - r_2 i_{L2} \quad (41)$$

$$i_{reg} = d_{S5}i_{L2} \quad (42)$$

The current and power delivered to the battery are calculated as Equations (43) and (44):

$$i_b = i_{L2} \tag{43}$$

$$P_b = -V_b i_{L2} \tag{44}$$

3 | DYNAMIC MODELLING OF THE CONVERTER

As mentioned in Section 2, the proposed converter includes four scenarios. Different control variables are required in each scenario to adjust the input source current and output voltage. In the first and second scenarios, one duty cycle is selected, while the third and fourth scenarios use two duty cycles. Therefore, in the first and second scenarios, V_o can be controlled directly, while the other state variable (i_{L1} or i_{L2}) is automatically adjusted according to the power of the converter operating point. In the third and fourth scenarios, V_o and i_{L2} and thus the battery current is directly controlled and the state variable corresponding to the input source (i_{L1}) is adjusted automatically. To obtain the dynamic model for each scenario, i_{L1}, i_{L2}, and V_o are selected as state variables. The state-space average model (SSAM) is then used in each scenario as follows:

First scenario: In this scenario, d_{S4} is selected as a control variable that controls V_o. SSAM is obtained as follows:

$$L_1 \dot{i}_{L1} = V_1 - (1 - d_{S4}) V_o - r_1 i_{L1} \tag{45}$$

$$C_o \dot{V}_o = (1 - d_{S4}) i_{L1} - I_o \tag{46}$$

Second scenario: Similar to the first scenario, this scenario uses d_{S3} to control V_o. Using SSAM, these equations are obtained:

$$L_2 \dot{i}_{L2} = V_b - (1 - d_{S3}) V_o - r_2 i_{L2} \tag{47}$$

$$C_o \dot{V}_o = (1 - d_{S3}) i_{L2} - I_o \tag{48}$$

Third scenario: In this scenario, using d_{T1} and d_{S3} as control variables, V_o and battery discharge power can be controlled. Since $d_{T1} = 1\text{-}d_{S1}$, the SSAM is obtained as follows:

$$L_1 \dot{i}_{L1} = \frac{1}{L_1 + L_2}(L_1 + L_2 d_{T1}) V_1 - (1 - d_{S3}) V_o - \frac{1}{L_1 + L_2}\left[(L_1 + L_2 d_{T1}) r_1 + L_1 (1 - d_{T1}) r_2\right] i_{L1} \tag{49}$$

$$L_2 \dot{i}_{L2} = \frac{L_2}{L_1 + L_2}(1 - d_{T1}) V_1 + d_{T1} V_b - (1 - d_{S3}) V_o - \frac{1}{L_1 + L_2}\left[L_2 (1 - d_{T1}) r_1 + (L_2 + L_1 d_{T1}) r_2\right] i_{L2} \tag{50}$$

$$C_o \dot{V}_o = (1 - d_{S3})(i_{L1} + i_{L2}) - I_o \tag{51}$$

Fourth scenario: In this scenario, i_{L1} and i_{L2} are equal. Therefore, i_{L1} and V_o are selected as state variables. d_{T2} and d_{S3} are control variables that control the battery charge power and V_o, respectively. SSAM for this scenario is as follows:

$$L_1 \dot{i}_{L1} = \frac{L_1}{L_1 + L_2}\left[V_1 - d_{T2} V_b - (1 - d_{T2} - d_{S3}) V_o - (r_1 + r_2) i_{L1}\right] \tag{52}$$

$$C_o \dot{V}_o = (1 - d_{T2} - d_{S3}) i_{L1} - I_o \tag{53}$$

According to the small-signal model [22], the input voltages, state variables, and duty cycles consist of two parts: DC values ($\bar{V}$,$\bar{X}$,$\bar{D}$) and perturbations ($\tilde{v}$,$\tilde{x}$,$\tilde{d}$) as follows:

$$V = \bar{V} + \tilde{v}, \quad x = \bar{X} + \tilde{x}, \quad d = \bar{D} + \tilde{d} \tag{54}$$

Assuming that the oscillations of the perturbations are negligible, by applying Equation (55) in Equations (45)–(53) and ignoring the second-order sentences, a small-signal model is obtained which it can be written in matrix form as follows:

$$\begin{aligned} \dot{\tilde{x}} &= A\tilde{x} + B\tilde{u} \\ \tilde{y} &= C\tilde{x} + D\tilde{u} \end{aligned} \tag{55}$$

In Equation (55), $\tilde{x}$, $\tilde{u}$ and $\tilde{y}$ are the vectors of state variables, control variables, and output, respectively. A, B, C and D are the matrixes of state, input, output, and feed-forward. Therefore, the small signal-model is obtained as a matrix for all scenarios as follows:

First scenario:

$$A = \begin{bmatrix} -\frac{r_1}{L_1} & \frac{\bar{D}_{S4} - 1}{L_1} \\ \frac{1 - \bar{D}_{S4}}{C_o} & -\frac{1}{R_o C_o} \end{bmatrix}, B = \begin{bmatrix} \frac{\bar{V}_o}{L_1} \\ -\frac{\bar{I}_{L1}}{C_o} \end{bmatrix} \tag{56}$$

$$\tilde{x} = \begin{bmatrix} \tilde{i}_{L1} \\ \tilde{v}_o \end{bmatrix}, C = \begin{bmatrix} 0 & 1 \end{bmatrix}, D = 0, \tilde{u} = \tilde{d}_{S4}, \tilde{y} = \tilde{v}_o$$

Second scenario:

$$A = \begin{bmatrix} -\frac{r_2}{L_2} & \frac{\bar{D}_{S3} - 1}{L_2} \\ \frac{1 - \bar{D}_{S3}}{C_o} & -\frac{1}{R_o C_o} \end{bmatrix}, B = \begin{bmatrix} \frac{\bar{V}_o}{L_2} \\ -\frac{\bar{I}_{L2}}{C_o} \end{bmatrix} \tag{57}$$

$$\tilde{x} = \begin{bmatrix} \tilde{i}_{L2} \\ \tilde{v}_o \end{bmatrix}, C = \begin{bmatrix} 0 & 1 \end{bmatrix}, D = 0, \tilde{u} = \tilde{d}_{S3}, \tilde{y} = \tilde{v}_o$$

Third scenario:

$$A=\begin{bmatrix} -\frac{L_1+L_2\bar{D}_{T1}}{L_1(L_1+L_2)}r_1-\frac{1-\bar{D}_{T1}}{L_1+L_2}r_2 & 0 & \frac{\bar{D}_{S3}-1}{L_1} \\ 0 & -\frac{1-\bar{D}_{T1}}{L_1+L_2}r_1-\frac{L_2+L_1\bar{D}_{T1}}{L_2(L_1+L_2)}r_2 & \frac{\bar{D}_{S3}-1}{L_2} \\ \frac{1-\bar{D}_{S3}}{C_o} & \frac{1-\bar{D}_{S3}}{C_o} & -\frac{1}{R_oC_o} \end{bmatrix}$$

$$B=\begin{bmatrix} \frac{L_2\bar{V}_1}{L_1(L_1+L_2)}-\frac{L_2r_1-L_1r_2}{L_1(L_1+L_2)}\bar{I}_{L1} & \frac{\bar{V}_o}{L_1} \\ -\frac{\bar{V}_1}{L_1+L_2}+\frac{\bar{V}_b}{L_2}-\frac{L_1r_2-L_2r_1}{L_2(L_1+L_2)}\bar{I}_{L1} & \frac{\bar{V}_o}{L_2} \\ 0 & -\frac{\bar{I}_{L1}+\bar{I}_{L2}}{C_o} \end{bmatrix} \tag{58}$$

$$\tilde{x}=\begin{bmatrix}\tilde{i}_{L1}\\ \tilde{i}_{L2}\\ \tilde{v}_o\end{bmatrix},\tilde{u}=\begin{bmatrix}\tilde{d}_{T1}\\ \tilde{d}_{S3}\end{bmatrix},\tilde{y}=\begin{bmatrix}\tilde{v}_o\\ \tilde{i}_{L2}\end{bmatrix},C=\begin{bmatrix}0 & 0 & 1\\ 0 & 1 & 0\end{bmatrix},D=0$$

Fourth scenario:

$$A=\begin{bmatrix} -\frac{r_1+r_2}{L_1+L_2} & \frac{\bar{D}_{T2}+\bar{D}_{S3}-1}{L_1+L_2} \\ \frac{1-\bar{D}_{T2}-\bar{D}_{S3}}{C_o} & -\frac{1}{R_oC_o} \end{bmatrix},$$

$$B=\begin{bmatrix} \frac{\bar{V}_o-\bar{V}_b}{L_1+L_2} & \frac{\bar{V}_o}{L_1+L_2} \\ -\frac{\bar{I}_{L1}}{C_o} & -\frac{\bar{I}_{L1}}{C_o} \end{bmatrix} \tag{59}$$

$$\tilde{x}=\begin{bmatrix}\tilde{i}_{L1}\\ \tilde{v}_o\end{bmatrix},\tilde{u}=\begin{bmatrix}\tilde{d}_{T2}\\ \tilde{d}_{S3}\end{bmatrix},\tilde{y}=\begin{bmatrix}\tilde{v}_o\\ \tilde{i}_{L2}\end{bmatrix},$$

$$C=\begin{bmatrix}0 & 1\\ 1 & 0\end{bmatrix},D=\begin{bmatrix}0 & 0\\ 0 & 0\end{bmatrix}$$

4 | CONTROL SYSTEM OF THE CONVERTER

As can be seen from Section 3, the control system in the first and second scenarios consists of one control loop, while the control system of the third and fourth scenarios consists of two control loops. For this proposed converter, an integral state feedback-based control method called the pole placement method [23] is used. The controllability matrix is defined as follows:

$$\Psi_C=\left[B\vdots AB\vdots A^2B\vdots\cdots\vdots A^{n+1}B\right] \tag{60}$$

If the matrix rank is complete (equal to n+2), the system becomes completely state-controllable. The value of n for the first and second scenarios is $n=1$. For the third and fourth scenarios, its value is $n=2$. Therefore, for the first and second scenarios, the rank Ψ_C should be 3 and for the third and fourth scenarios, it should be 4. Now, for each scenario, additional integral states are considered as follows:

First and second scenarios:

$$\dot{q}(t)=r(t)-y(t)=r(t)-\tilde{v}_o(t) \tag{61}$$

Third and fourth scenarios:

$$\begin{aligned}\dot{q}_1(t)&=r_1(t)-y_1(t)=r_1(t)-\tilde{v}_o(t)\\ \dot{q}_2(t)&=r_2(t)-y_2(t)=r_2(t)-\tilde{i}_{L2}(t)\end{aligned} \tag{62}$$

The state and output equations are rewritten according to the new integral states as follows:

$$\begin{aligned}\begin{bmatrix}\dot{\tilde{x}}(t)\\ \dots\\ \dot{q}(t)\end{bmatrix}&=\begin{bmatrix}A & \vdots & 0\\ \dots & \vdots & \dots\\ -C & \vdots & 0\end{bmatrix}\begin{bmatrix}\tilde{x}(t)\\ \dots\\ q(t)\end{bmatrix}+\begin{bmatrix}B\\ \dots\\ 0\end{bmatrix}\tilde{u}(t)+\begin{bmatrix}0\\ \dots\\ I\end{bmatrix}r(t)\\ \tilde{y}(t)&=\begin{bmatrix}C\vdots 0\end{bmatrix}\begin{bmatrix}\tilde{x}(t)\\ \dots\\ q(t)\end{bmatrix}\end{aligned} \tag{63}$$

In Equation (65), the vector $r(t)$ is the input reference vector defined for each scenario as follows:

First and second scenarios:

$$r(t) = \left[V_{o,ref}\right] \tag{64}$$

Third and fourth scenarios:

$$r(t) = \left[\begin{array}{cc} V_{o,ref} & i_{L2,ref} \end{array}\right]^T \tag{65}$$

The controllability matrix for the system defined in Equation (63) ($\bar{\Psi}_C$) can be arranged as follows:

$$\bar{\Psi}_C = \begin{bmatrix} B & \vdots & A\Psi_C \\ \dots & \vdots & \dots \\ 0 & \vdots & -C\Psi_C \end{bmatrix} = \underbrace{\begin{bmatrix} B & \vdots & A \\ \dots & \vdots & \dots \\ 0 & \vdots & -C \end{bmatrix}}_{M} \begin{bmatrix} I & \vdots & 0 \\ \dots & \vdots & \dots \\ 0 & \vdots & \Psi_C \end{bmatrix} \tag{66}$$

If Ψ_C is considered a complete rank, the system defined in Equation (63) is completely controllable if and only if the rank of the matrix M is $2n+2$. Therefore, there is a matrix K that satisfies the following equation:

$$\tilde{u}(t) = -K \begin{bmatrix} \tilde{x}(t) \\ \dots \\ q(t) \end{bmatrix} = -\begin{bmatrix} K_x & \vdots & K_q \end{bmatrix} \begin{bmatrix} \tilde{x}(t) \\ \dots \\ q(t) \end{bmatrix} \tag{67}$$

By placing Equation (67) in (63) the following equation is obtained:

$$\begin{bmatrix} \dot{\tilde{x}}(t) \\ \dots \\ \dot{q}(t) \end{bmatrix} = \begin{bmatrix} A - BK_x & \vdots & -BK_q \\ \dots & \vdots & \dots \\ -C & \vdots & 0 \end{bmatrix} \begin{bmatrix} \tilde{x}(t) \\ \dots \\ q(t) \end{bmatrix} + \begin{bmatrix} 0 \\ \dots \\ I \end{bmatrix} r(t) \tag{68}$$

The purpose of the problem is to find the vector $\tilde{u}(t)$ through the matrix K so that the eigenvalues of the closed-loop system are in the desired locations. To do this, the MATLAB software control systems toolbox is used. Figure 7 shows a block diagram of the pole placement control method in four scenarios in which L_2 current and V_o track the reference values of $I_{L2,ref}$ and $V_{o,ref}$, respectively. Figure 8 shows a flowchart of a control system designed for scenarios. First, i_{L1}, V_1, I_o, and V_o are sampled. In the scenario diagnosis unit, the operation scenario of the proposed converter is detected by comparing the input power (P_1) and output power (P_o). Besides, battery conditions such as $V_{b,min}$ and $V_{b,max}$ are important for defining scenarios. For example, when $P_o \le P_1$ and $V_b < V_{b,max}$, V_1 supply the load and charge the battery, this is called the fourth scenario. Depending on the diagnosis unit, different scenarios are detected that operate based on the corresponding block diagram shown in Figure 7

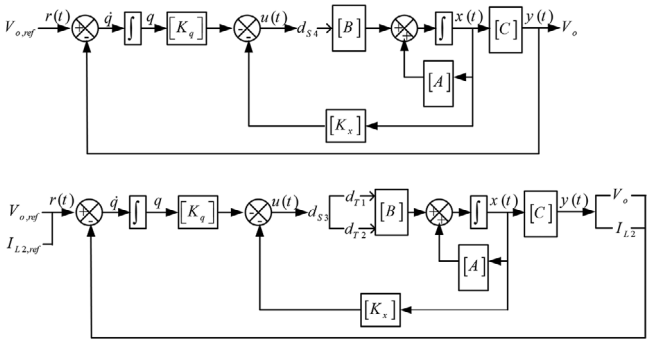

FIGURE 7 Block diagram of the pole placement control method; (a) The first and second scenarios, (b) The third and fourth scenarios

5 | DESIGN OF THE PROPOSED CONVERTER

To prepare a laboratory prototype of the proposed three-port converter, components such as L_1 and L_2 must be designed in such a way that the converter can operate in CCM. For this purpose, the average current of the inductor must be more than half of its current ripple. Besides, C_o is designed to minimize the output voltage ripple. Table 1 presents the minimum values of L_1, L_2, and C_o in each scenario.

The converter is designed according to these specifications: $V_1 = 30$ V, $V_b = 24$ V, $V_o = 96$ V, $P_o = 200$ W and switching frequency $f = 40$ kHz. The values of duty cycles in each scenario are as follows: the first scenario $d_{S4} = 0.71$, the second scenario $d_{S3} = 0.77$, the third scenario $d_{S3} = 0.75$ and $d_{T1} = 0.86$, the fourth scenario $d_{S3} = 0.49$ and $d_{T2} = 0.3$. According to the above specifications and using the relationships in Table 1 $L_1 = L_2 = 200$ μH and $C_o = 100$ μF are selected for the implementation of the laboratory prototype.

6 | DEVICES VOLTAGE AND CURRENT STRESSES

PVS of the devices is one of the important factors that is considered in the design of the converter and affects its cost and size. This factor increases with increasing converter voltage gain. So, another factor called normalized PVS (NPVS), which is defined as NPVS = PVS/V_o, is considered. Table 2 shows the PVS and NPVS of the devices and the scenario in which PVS occurs. Figure 9 shows the NPVS of the semiconductors in terms of different duty cycles, $V_1 = 30$ V, and $V_b = 24$ V. This figure shows that for all duty cycles, the NPVS of S_1, S_2, S_4, T_2, and D_2 is less than 1, which means that the PVS in these semiconductors is less than V_o.

For S_3 and S_5, PVS is equal to the output voltage. For duty cycles close to 1, the NPVS on T_1 is higher than 1, and the converter is not used in these duty cycles. Also, the NPVS on D_1 for $d_{S3} < 0.25$ is higher than 1 which the

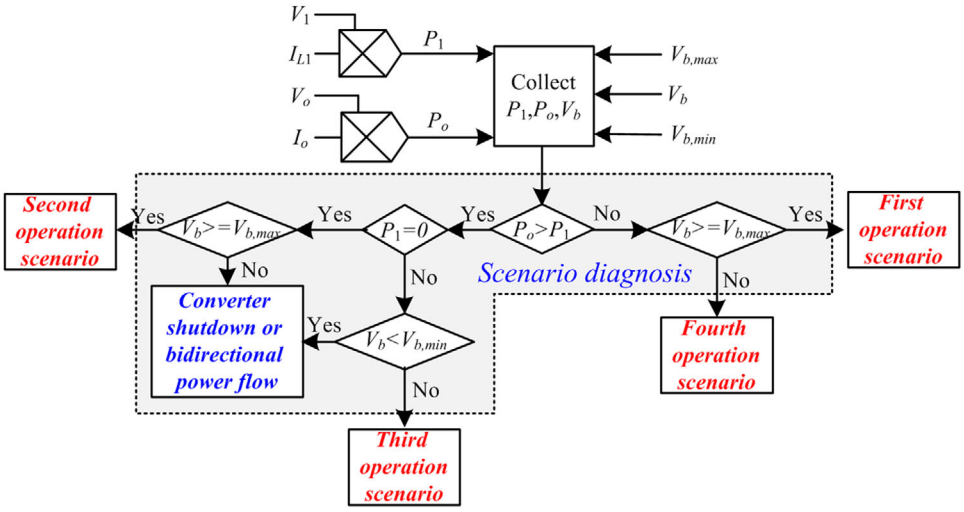

FIGURE 8 Flowchart of the control system

TABLE 1 $L_{1,\min}$, $L_{2,\min}$ and $C_{o,\min}$ values for each scenario

Scenario	Inductors		Capacitor
	$L_{1,min}$	$L_{2,min}$	$C_{o,min}$
First	$\frac{d_{S4}(1-d_{S4})^2 R_o}{2f}$	—	$\frac{d_{S4}}{R_o f \Delta v_{Co}\%}$
Second	—	$\frac{d_{S3}(1-d_{S3})^2 R_o}{2f}$	$\frac{d_{S3}}{R_o f \Delta v_{Co}\%}$
Third	$\frac{L_1 L_2}{L_2 V_1 + L_1 V_b} \geq \frac{R_o(1-d_{S3})^2(d_{S3}+d_{T1}-1)}{f(V_1+d_{T1}V_b)}$		$\frac{d_{S3}+d_{T1}-1}{R_o f \Delta v_{Co}\%}$
Fourth	$L_1 + L_2 \geq \frac{R_o V_1 d_{S3}(1-d_{T2}-d_{S3})^2}{2f(V_1-d_{T2}V_b)}$		$\frac{d_{S3}}{R_o f \Delta v_{Co}\%}$

TABLE 2 PVS, NPVS and related scenario

S/D	PVS	NPVS	Which scenario
S_1	$V_o - V_b$	$\frac{V_1+(2d_{S3}+d_{T1}-2)V_b}{V_1+d_{T1}V_b}$	3rd
S_2	$V_o - \frac{19V_1-16V_b}{3}$	$\frac{(19-16d_{S3})V_b-19(1-d_{S3})V_1}{3V_b}$	2nd
S_3	V_o	1	2nd, 3rd, 4th
S_4	$\frac{3}{4}(V_o-V_b)$	$\frac{3[V_1-(1-d_{S4})V_b]}{4V_1}$	1st
S_5	V_o	1	1st,3rd
T_1	$\frac{1}{2}(V_o+V_1)-V_b$	$\frac{(2-d_{T2}-d_{S3})V_1}{2(V_1-d_{T2}V_b)} - \frac{(2-d_{T2}-2d_{S3})V_b}{2(V_1-d_{T2}V_b)}$	4th
T_2	$V_o - V_b$	$\frac{V_1+(2d_{S3}+d_{T1}-2)V_b}{V_1+d_{T1}V_b}$	2nd, 3rd, 4th
D_1	$\frac{16}{3}(V_1-V_b)$	$\frac{16(1-d_{S3})(V_1-V_b)}{3V_b}$	2nd
D_2	$\frac{1}{2}(V_o+V_1)$	$\frac{(2-d_{T2}-d_{S3})V_1-d_{T2}V_b}{2(V_1-d_{T2}V_b)}$	4th
C_o	V_o	1	All

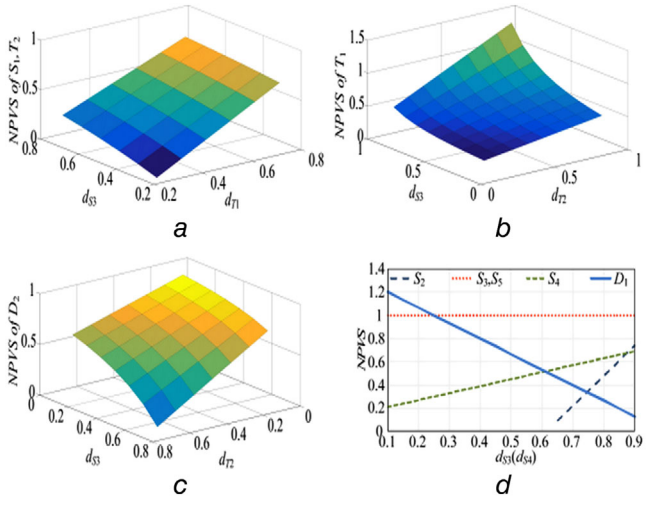

FIGURE 9 NPVS on semiconductors ($V_1 = 30$ V and $V_b = 24$ V); (a) T_2 and S_1, (b) T_1, (c) D_2, (d) S_2, S_3, S_4, S_5 and D_1

converter is not used in these duty cycles. Another factor that extremely affects the size and cost of the converter is the current stress of the components. To analyse the power loss of the converter, at first, the average and RMS current stress of the components should be calculated. These values can be calculated using the RMS and average values definitions. Because of avoiding redundant calculations, for instance, the current stress of the devices is studied only in the second scenario. For other scenarios, these values can be calculated easily using relevant definitions. Using Figure 3 and Equation (12), the average current of L_2 and T_1 is determined as follows:

$$I_{L2} = I_{T1} = \frac{I_o}{1 - d_{S3}} \tag{69}$$

In this scenario, S_3 is turned on only in subinterval I. So, for its average current, it can be said:

$$I_{S3} = d_{S3} I_{L2} = \frac{d_{S3}}{1 - d_{S3}} I_o \tag{70}$$

Furthermore, the body diodes of S_4 and S_5 conducts the same current in subinterval II. This equation states their average current:

$$I_{DS4} = I_{DS5} = (1 - d_{S3}) I_{L2} = I_o \tag{71}$$

Then, the RMS current of the devices according to the RMS definition. For switch S_3:

$$i_{S3,rms} = \sqrt{\frac{1}{T}\int_0^{d_{S3}T} I_{L2}^2 dt} = \sqrt{\frac{1}{T}\left(\frac{I_o}{1 - d_{S3}}\right)^2 d_{S3}T}$$
$$= \frac{\sqrt{d_{S3}}}{1 - d_{S3}} I_o \tag{72}$$

Similarly, for switches S_4 and S_5, the following equation can be written:

$$i_{S4,5rms} = \sqrt{\frac{1}{T}\int_{d_{S3}T}^{T} I_{L2}^2 dt} = \sqrt{\frac{1}{T}\int_{d_{S3}T}^{T} \left(\frac{I_o}{1 - d_{S3}}\right)^2 dt}$$
$$= \frac{I_o}{\sqrt{1 - d_{S3}}} \tag{73}$$

For capacitor C_o, the RMS current is determined as follows:

$$i_{Co,rms} = \sqrt{\frac{1}{T}\left(\int_0^{d_{S3}T} (-I_o)^2 dt + \int_{d_{S3}T}^{T} (I_{L2} - I_o)^2 dt\right)}$$
$$= \sqrt{\frac{d_{S3}}{1 - d_{S3}}} I_o \tag{74}$$

Based on the RMS definition, L_2 RMS current is calculated as follows:

$$i_{L2,rms} = \sqrt{\frac{1}{T}\left[\int_0^{d_{S3}T}\left(\frac{i_2 - i_1}{d_{S3}T}t + i_1\right)^2 dt + \int_{d_{S3}T}^{T}\left(\frac{i_1 - i_2}{(1 - d_{S3})T}t + \frac{i_2 - d_{S3} i_1}{1 - d_{S3}}\right)^2 dt\right]} \tag{75}$$

In Equation (74), i_2 and i_1 denote the maximum and minimum values of the inductor current, respectively. After some simplification, Equation (74) can be rewritten as Equation (76):

$$i_{L2,rms} = i_{T1,rms} = \sqrt{\left(\frac{I_o}{1 - d_{S3}}\right)^2 + \frac{1}{12}\left(\frac{d_{S3} V_b}{f L_2}\right)^2} \tag{76}$$

7 | COMPARISON STUDY

In this section, the proposed converter is compared with other three-port converters in the literature. The capabilities of bidirectional power flow, individual or simultaneous power transfer of sources, number of used components (switch, diode, inductor and capacitor), capabilities of voltage step-up, PVS on semiconductors etc., are selected as comparison factors and listed in Table 3 Among the structures presented in the table, only the structure in [15, 22, 23, 27] and the proposed converter have bidirectional power flow capability, which is one of the most important advantages of the proposed structure.

Another important advantage of the proposed structure is the simultaneous transfer of power from input sources, which can be seen in other structures in the table except for the converter in [22, 24, 27]. In the proposed converter, the energy storage device can be recharged by another source, a feature that can also be seen in the converters of [19, 22–25, 27]. The number of components used in the proposed structure is the same as the number of components in the structure in [18, 19, 26]. The

TABLE 3 Comparison of the proposed converter with other three-port converters in the literature

Parameter	Structures												
	[15]	[16]	[17]	[18] with $n_2/n_1 = 2.35$	[19]	[22]	[23] with $n = 2.4$	[24] with $n = 0.35$	[25] with $n = 1.9$, $n' = 3.8$	[26] with $n = 1$	[27]	[28] with $n = 1$	Proposed
Bidirectional	✓	✗	✗	✗	✗	✓	✓	✗	✗	✗	✓	✗	✓
Simultaneous power transfer	✓	✓	✓	✓	✓	✗	✓	✗	✓	✓	✗	✓	✓
Independent power transfer	✗	✗	✓	✗	✗	✗	✓	✓	✓	✗	✓	✗	✓
Battery charging by another input	✗	✗	✗	✗	✓	✓	✓	✓	✓	✗	✓	✗	✓
No. of switches	4	2	2	2	3	2	6	4	2	2	3	2	7
No. of diodes	2	3	5	3	5	1	2	5	2	4	–	4	2
No. of inductors	2	2	2	3	2	2	1	1	1	2	2	3	2
No. of capacitors	1	4	5	4	2	3	–	1	4	4	3	5	1
No. of components	9	11	14	12	12	8	9	11	9	12	8	14	12
PVS on switches ($V_1 = 30$ V, $V_b = 24$ V, $V_o = 96$ V)	S_1: V_1 S_2: V_b T_0, Q_0: V_o	NA	$\frac{V_o}{4}$	$\frac{V_o}{2+\frac{n_2}{n_1}}$	S_1: V_o S_2, S_3: V_b	NA	$S_{1,2}$: $0.5V_o$ S_3: V_1-V_b S_4: V_o S_{a1} : $(1+\frac{1}{n})V_o + \frac{V_{IN}}{n}$ S_{a2} : $V_o + \frac{V_b}{n}$	S_1: V_1-V_b S_2: V_o– V_b S_3: V_o S_4: $(1+n)V_o$-nV_{IN}	S_1 : $\frac{n-1}{n+n'}V_o$ S_2 : $V_b + \frac{nV_1}{n-1}$	S_1 : $\frac{V_1 - V_2}{d_2}$ S_2 : $\frac{V_1}{1-d_2}$		$\frac{V_1}{1-\frac{V_o}{4+2nd}}$	Reported in Table 2
	S_1: 30V S_2: 24 V T_0, Q_0: 96V	NA	24 V	22.07 V	S_1: 96V S_2, S_3: 24 V	NA	$S_{1,2}$: 48 V S_3: 6 V S_4: 96 V S_{a1}: 137.7 V S_{a2}: 106 V	S_1: 6V S_2: 72 V S_3: 96 V S_4: 115.6V	S_1: 15.16 V S_2: 87.33 V	S_1: 42.86 V S_2: 34.88 V	50.85 V	18.11 V	S_1: 72 V, S_2: 34 V, S_3: 96 V, S_4: 54 V, S_5: 96 V, T_1: 39 V, T_2: 72 V
PVS on diodes ($V_1 = 30$ V, $V_b = 24$ V, $V_o = 96$ V)	D_1: V_1 D_2: V_b	NA	$D_{1,\ldots,4}$: $0.25V_o$ D_o: $0.5V_o$	D_1 : $\frac{V_o}{2+\frac{n_2}{n_1}}$ $D_{2,o}$: $\frac{1+\frac{n_2}{n_1}}{2+\frac{n_2}{n_1}}V_o$	D_3: V_o D_4, D_5: V_b	NA	D_1: V_b-V_1 D_2: V_b	D_1: V_b-V_1 $D_{2,3}$: V_b D_4: nV_b D_5: V_o	D_o : $\frac{1+n'}{n+n'}V_o$ D_d : $V_b - \frac{(nd+n')V_1}{(n-1)(1-d)}$	D_1 : $\frac{(n+1)d_2-1}{1-d_2}V_1 + \frac{V_2}{d_2}$ $D_{2,3,o}$: $\frac{1+n}{1-d_2}V_1$	–	$\frac{V_o}{2+nd}$	Reported in Table 2
	D_1: 30V D_2: 24 V	NA	$D_{1,\ldots,4}$: 24V D_o: 48 V	D_1: 22.07 V $D_{2,o}$: 73.93 V	D_3: 96V D_4, D_5: 24 V	NA	D_1: 6 V D_2: 24 V	D_1: 6V $D_{2,3}$: 24 V D_4: 8.4 V D_5: 96V	$D_o = 80.84$ $D_d = 251.95$ V	D_1: 146.31 V $D_{2,3,o}$: 69.77 V	–	36.23 V	D_1: 32 V D_2: 63 V

(Continues)

TABLE 3 (Continued)

Parameter	Structures												
	[15]	[16]	[17]	[18] with $n_2/n_1 = 2.35$	[19]	[22]	[23] with $n = 2.4$	[24] with $n = 0.35$	[25] with $n = 1.9$, $n' = 3.8$	[26] with $n = 1$	[27]	[28] with $n = 1$	Proposed
Step-up	✓	✓	✓	✓	✓	✓	✓	✓	✓	✓	✓	✓	✓
Extension	✓	✓	✓	✓	NA	NA	NA	NA	NA	NA	NA	NA	✓
Common ground	✓	✓	✗	✗	✗	✗	✓	✓	✗	✓	✗	✗	✓
No. of scenarios	1	1	1	1	3	1	4	4	3	1	1	1	4
Efficiency in rated power (%)	93.5 (discharging) 95.5 (charging)	90	91	95.9	91-93	NA	97.5	97.22	95.38	95.4	93.2 (boo 94.5 (buc	96.35	91.7 (1st scenario), 95 (2nd scenario) 94 (3rd scenario), 92.4 (4th scenario)

structures of [17, 28] use more components and the structures of [15, 16, 22–25, 27] use fewer components than the proposed structure. PVS of the switches and diodes is another factor that should be compared between the structures of Table 3 To have a better comparison between the proposed converter and the converters in literature in terms of PVS, it is supposed that all the converters have the same conditions ($V_1 = 30$ V, $V_b = 24$ V, $V_o = 96$ V). Considering this, the values for PVS on semiconductors have been included in Table 3 As can be seen, only the switches S_3 and S_5 experience the voltage stress of V_o, while the other switches of the proposed converter have PVS lower than the output voltage. The switches T_0 and Q_0 in [15], S_1 in [19], S_4 in [23], and S_3 in [24] have also the PVS equals to V_o. it is noticeable that the switches S_{a1} and S_{a2} in [23] and S_4 in [24] endure the PVS higher than the output voltage. The PVS on diodes of the proposed converter is lower than V_o. The diodes of the other structures such as D_3 in [19] and D_5 in [24] experience the PVS equal to V_o. Furthermore, the PVS on diode D_d in [25] and D_1 in [26] is higher than the proposed converter and these diodes must endure the voltage stress more than V_o.

All structures in the table have the voltage step-up ability and expansion of the number of inputs. In DC-DC converters, where there is a common ground between the input and output ports, they have high safety and fewer protection problems and electromagnetic interference. Besides, there is no addition dv/dt between input and output grounds [19]. Among the structures in the table, only the structures of [15, 16, 23, 24, 26], and the proposed converter have common ground characteristics. The last row of the Table 3 compares the efficiency of the proposed converter with other converters. As it is clear, the efficiency of the proposed converter in the first to fourth scenarios varies between 91.7–95%, which is higher than the efficiency of the converters in [16, 17, 19, 27]. Furthermore, the proposed converter efficiency is almost equal to the efficiency of the converters in [15, 18, 25, 26]. As the main results of the comparisons, the proposed converter contains positive points in terms of the main quality factors. The positive points can be considered with the acceptable number of used components, the possibilities of bidirectional power flow, simultaneous and individual power transfer of input sources, charging the battery by another input source, the existence of common ground, and its high efficiency. It is worth noting that none of the converters compared at the same time have these advantages, and each of them has one or two drawbacks compared to the proposed converter. So, the proposed converter can be presented as a step-up converter with significant positive points for hybrid systems.

8 | THERMAL AND LOSS ANALYSIS

Power components dissipate a large amount of power which is converted to heat and results in increasing the junction temperature (T_j) of the component. This temperature should not be higher than the maximum junction temperature (T_{jmax}), since, permanent damage to the device will occur. In a semiconductor, the dissipated heat is conducted away from the junction to the case, from the case to the heat sink, and from the heat sink to

the ambient. The rise in the junction temperature is determined by [31]:

$$\Delta T_{ja} = T_j - T_a = R_{ja}P_d = (R_{jc} + R_{cs} + R_{sa})P_d \quad (77)$$

In Equation (77), P_d is the power dissipation, R_{ja}, R_{jc}, R_{cs}, and R_{sa} are the thermal resistances of junction-to-ambient, junction-to-case, case-to-sink, and sink-to-ambient, respectively. From Equation (77), the maximum power dissipation is as follows:

$$P_{d\max} = \frac{T_{j\max} - T_a}{R_{ja}} \quad (78)$$

T_{jmax}, R_{jc}, and the maximum safe power dissipation $P_{d0} = P_{d(\text{rated})}$ of semiconductor components rated at the case temperature $T_c = T_{a0} = 25\ ^\circ\text{C}$ are given in the datasheets. It is noticed that $T_c = T_{a0} = 25\ ^\circ\text{C}$ is for the conditions in which the cooling of the case is ideal and thermal resistance between the case and ambient is zero. In these situations, the rated power is determined as follows:

$$P_{d0} = P_{d(rated)} = \frac{T_{j\max} - T_{d0}}{R_{jc}} \quad (79)$$

The power MOSFETs used in the proposed converter are of type IRFP260N with $T_{jmax} = 175\ ^\circ\text{C}$, $T_a = 30\ ^\circ\text{C}$, $R_{jc} = 0.5\ ^\circ\text{C/W}$, $R_{cs} = 0.24\ ^\circ\text{C/W}$ and $R_{sa} = 5\ ^\circ\text{C/W}$. For this MOSFET, the maximum power dissipation is achieved $P_{d\max} = 25.26$ W. For IGBTs of type BUP400 with $T_{jmax} = 150\ ^\circ\text{C}$, $T_a = 30\ ^\circ\text{C}$, $R_{jc} = 1.25\ ^\circ\text{C/W}$, $R_{cs} = 1\ ^\circ\text{C/W}$ and $R_{sa} = 5\ ^\circ\text{C/W}$, the value of $P_{d\max} = 16.55$ W is calculated. The power diodes MUR1560 used for the proposed converter with characteristics of $T_{jmax} = 175\ ^\circ\text{C}$, $T_a = 30\ ^\circ\text{C}$, $R_{jc} = 1.5\ ^\circ\text{C/W}$, $R_{cs} = 1\ ^\circ\text{C/W}$, and $R_{sa} = 5\ ^\circ\text{C/W}$, maximum power dissipation is determined as $P_{d\max} = 19.33$ W.

A comprehensive study of the efficiency is described here. For this purpose, the MOSFET switches are modelled with an ON-state resistance (r_{DS}) and the IGBT switches are modelled with a resistance (r_{CE}) in series with a DC voltage source (V_{CE}). The diodes are modelled with a resistance (r_D) in series with a DC voltage source representing voltage drop (V_F). The equivalent series resistance (ESR) of inductors (r_L) and capacitors (r_C) is also considered. The calculation of the efficiency for all scenarios is similar. So, to avoid redundant equations, for instance, the efficiency is calculated only for the second scenario. The total power loss (P_{Loss}) is considered as follows:

$$P_{Loss} = P_{rL} + P_{rC} + P_S + P_D \quad (80)$$

P_{rL}, P_{rC}, P_S, and P_D designate the losses correlated with ESRs of inductors, ESRs of capacitors, switches, and diodes, respectively. The ESR losses of inductors are evaluated as follows:

$$P_{rL} = P_{rL2} = r_2 i^2_{L2,rms} \quad (81)$$

For efficiency study, the current ripple of the inductors is neglected. Consequently, the RMS values of inductors currents are equal to average values. So, according to Equation (69), the currents through inductors are approximated as below:

$$i_{L2,rms} = \frac{I_o}{1 - d_{S3}} \quad (82)$$

Substituting Equation (82) in (81), the ESR losses of the inductor is calculated. The capacitor ESR losses are written as follows:

$$P_{rC} = P_{rCo} = r_{Co} i^2_{Co,rms} \quad (83)$$

The RMS value of the current through the capacitor is given in Equation (74). Substituting this value in Equation (83), the ESR losses of the capacitor are obtained. The power losses of the switches are expressed as follows:

$$P_S = P_{rDS} + P_{rCE} + P_{VCE} + P_{SW} \quad (84)$$

In Equation (84), P_{rDS}, P_{rCE}, and P_{VCE} indicate the conduction losses of the switches. P_{SW} represents the switching losses of the switches. P_{rDS} and P_{rCE} are calculated as follows:

$$P_{rDS} = r_{DS3} i^2_{S3,rms} + r_{DS4} i^2_{S4,rms} + r_{DS5} i^2_{S5,rms} \quad (85)$$

$$P_{rCE} = r_{CET1} i^2_{T1,rms} \quad (86)$$

$i_{S3,rms},\ldots,i_{S5,rms}$ are the RMS values of the currents through the switches which are given in Equations (72) and (73). P_{VCE} for the switch T_1 is calculated as follows:

$$P_{VCE} = V_{CET1} I_{T1} \quad (87)$$

Besides, the switching losses (P_{SW}) are evaluated as follows:

$$P_{SW} = \sum_{i=1}^{4} \frac{1}{6} f v_{Si} I_{Si} (t_{on,i} + t_{off,i}) \quad (88)$$

In Equation (88), f, v_S, and I_s are the switching frequency, voltage across the power switch S, and the average current of the switch. t_{on} and t_{off} denote respectively the current rise and fall times of switches given in the switch datasheet. Eventually, the efficiency of the converter is calculated as follows:

$$\eta = \frac{P_o}{P_o + P_{Loss}} \times 100 = \frac{V_o I_o}{V_o I_o + P_{Loss}} \times 100 \quad (89)$$

9 | EXPERIMENTAL RESULTS

As mentioned in Section 2, the performance of the proposed converter is generally divided into two modes of unidirectional and bidirectional power flow. On the other hand, the unidirec-

FIGURE 10 Laboratory image of the converter with experimental setup

tional mode has four operation scenarios. In this section, for instance, the experimental results of the proposed converter are presented in three scenarios related to unidirectional mode and also in bidirectional mode. Figure 10 shows a laboratory sample of the proposed converter with an experimental setup. The parameters used in the proposed converter are given in Table 4

9.1 | Unidirectional power flow operation

Depending on the status of the battery usage, this mode is divided into four scenarios. For instance, the experimental results for three scenarios are given below:

9.1.1 | First scenario

In this scenario, d_{S4} is used to adjust V_o and its value is set to $d_{S4} = 0.71$. The experimental waveforms of the converter are shown in Figure 11 As Figure 11 shows, V_o is set to 96 V. The experimental waveforms v_{S4} and v_{S5} are shown in Figure 11b c. It is clear from Figure 11b that the PVS on S_4 is around 55 V. Besides, according to Figure 11c PVS on S_5 is about 95 V. These two switches withstand the maximum voltage stress in this scenario. Figure 11d shows the experimental waveform of i_{L1}. According to this figure, the average value of the current is equal to 7.2 A and the peak-to-peak current ripple is equal to 2.3 A. Based on these data, it can be said that the current ripple of V_1 is about 32% and the power delivered by this source is equal to 216 W.

9.1.2 | Second scenario

In this scenario, d_{S3} is used to adjust the output voltage. The value of this duty cycle is set to 0.77. The experimental waveforms of the converter are shown in Figure 12 V_o waveform is shown in Figure 12a which is similar to the first scenario showing the voltage 96 V on C_o. The voltage waveform of T_2 is shown in Figure 12b This figure indicates that the PVS on T_2 is 74 V. This switch withstands the maximum voltage stress in this scenario. Figure 12c shows the voltage waveform across D_1. It is clear from this figure that the PVS on D_1 is about 32 V, which is the maximum stress that D_1 can withstand in the proposed converter. As can be seen, i_b is continuous and the average value and peak-to-peak current ripple are 9 and 2.1 A, respectively.

9.1.3 | Third scenario

In this scenario, the V_o and i_{L2} are regulated by d_{T1} and d_{S3}, respectively, and for this purpose, $d_{T1} = 0.86$ and $d_{S3} = 0.75$. V_o waveform is shown in Figure 13a As this figure shows, similar to the previous scenarios, the amount of V_o has been stabilized by adopting the above duty cycles in the 96 V. Figure 13b c shows the experimental waveforms of v_{S1} and v_{S5}.

As can be seen from the figures, the PVS of these switches is 74 and 95 V, respectively. S_1 withstands the maximum voltage stress in this scenario. In addition to this scenario, S_5 also experiences maximum voltage stress equal to this value in the first scenario. The battery discharge current is shown in Figure 13d It can be seen that the average value of this current is about 3.6A. In this scenario, the battery power is about 85.7 W.

TABLE 4 Parameters of the proposed converter

Parameter	Value or part number		Parameter	Value or part number	
V_1	30 V		C_o	100 μF	Electrolytic
V_2	24 V (two 12 V, 7 Ah batteries in series)				
			P_o	200 W	
L_1, L_2	200 μH	Ferrite cores EE-42/21/15	V_o	96 V	
Diodes	MUR1560		S_2–S_5	MOSFET IRFP260N	
f	40 kHz		T_1, T_2, S_1	IGBT BUP400	

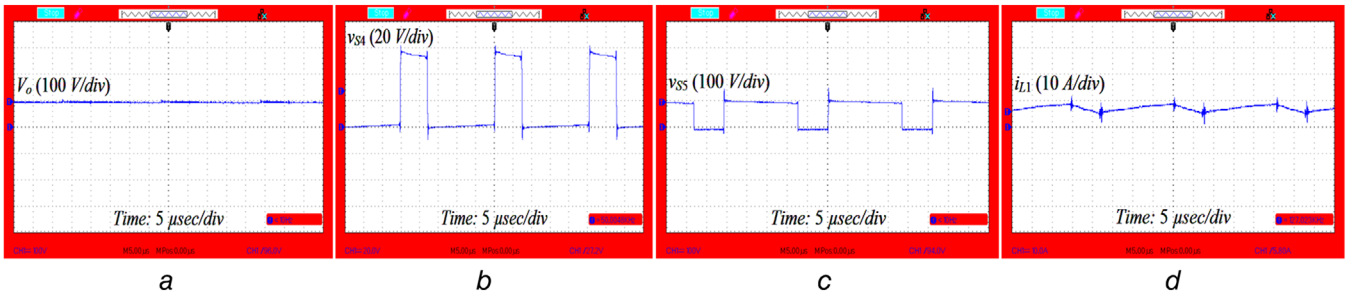

FIGURE 11 Experimental waveforms in the first scenario; (a) V_o, (b) switch S_4 voltage, (c) switch S_5 voltage, (d) inductor L_1 current

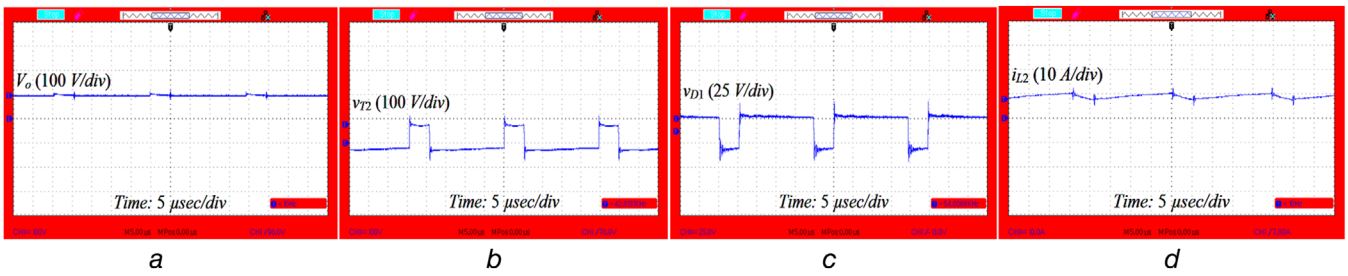

FIGURE 12 Experimental waveforms in the second scenario; (a) V_o, (b) switch T_2 voltage, (c) diode D_1 voltage (d) inductor L_2 current

9.2 | Bidirectional power flow operation

In this mode, V_1 is disabled and therefore L_1 is not used at all. The duty cycle d_{S5} is used to control L_2 current, which is the same as the battery current, and for this purpose, $d_{S5} = 0.26$. The experimental waveforms in the bidirectional mode are shown in Figure 14 Figure 14a b shows L_2 current and the battery charge current. These two figures show that the current of the battery and the inductor are equal and in opposite directions. The average value of these two currents is about 2 A. Figure 14c shows the average voltage of the battery. As can be seen, the average voltage of the battery is higher than 24 V, which indicates that the battery is charged.

Figure 15a and b illustrate the converter operation during the transient time when the operating scenarios are switched between the first and third scenarios. At first, the output port (R_L) is supplied by half of the nominal power and the port V_1 provides the load required power (first scenario). In other words, it is clear from Figure 15b that the battery is not used in this case and the whole power of the load is provided by the L_1 current. Then, a sudden-step change in the output power occurs from half load to full load. Therefore, L_1 current is increased compared to the first scenario and the battery port (V_b) is responsible for compensating the rest of the load power. As a result, the converter operates in third scenario. It is obvious from these figures that due to closed-loop control of the system, the output voltage is constant during these transitions and its variations are negligible.

The efficiency curves versus different output powers [105–200 W] for each scenario are depicted in Figure 16 Based on this figure, the converter efficiency in the 1st scenario is the lowest and in the 2nd scenario is the highest value. The maximum efficiency for the 1st to 4th scenario is 93%, 96.75%, 95% and 94.33%, respectively. The full load efficiency values are mentioned in Table 3.

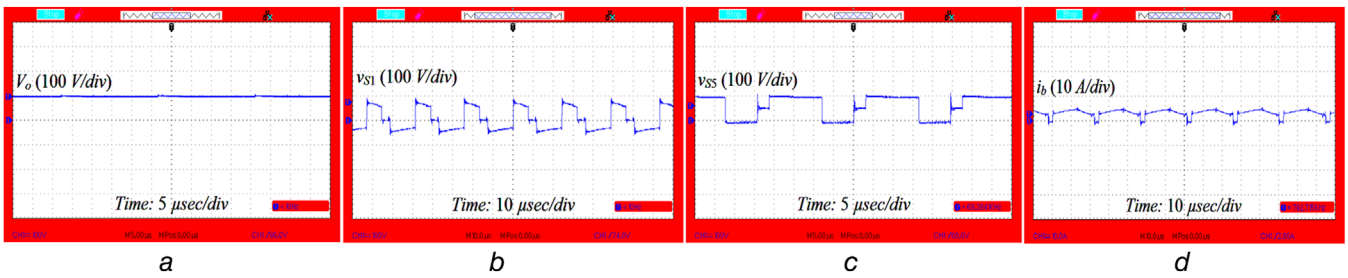

FIGURE 13 Experimental waveforms in the third scenario; (a) V_o, (b) switch S_1 voltage, (c) switch S_5 voltage (d) battery current

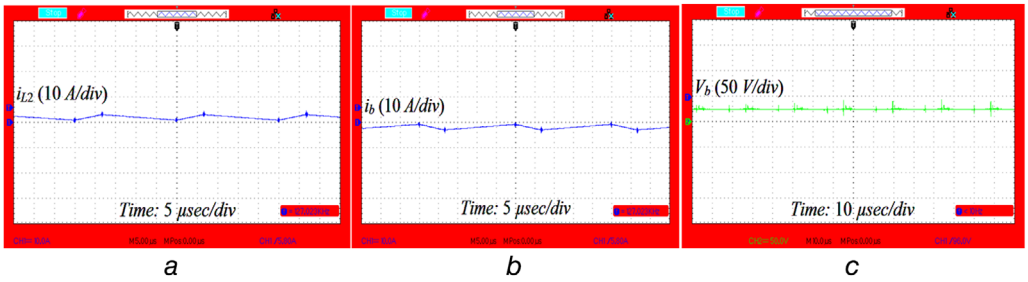

FIGURE 14 Experimental waveforms in the bidirectional operation; (a) inductor L_2 current, (b) battery current, (c) battery voltage

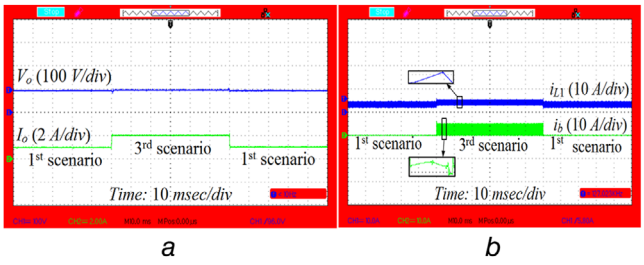

FIGURE 15 Experimental waveforms during the transition between the first and third scenarios; (a) output voltage (V_o) and current (I_o), (b) current of inductor L_1 (i_{L1}) and battery (i_b)

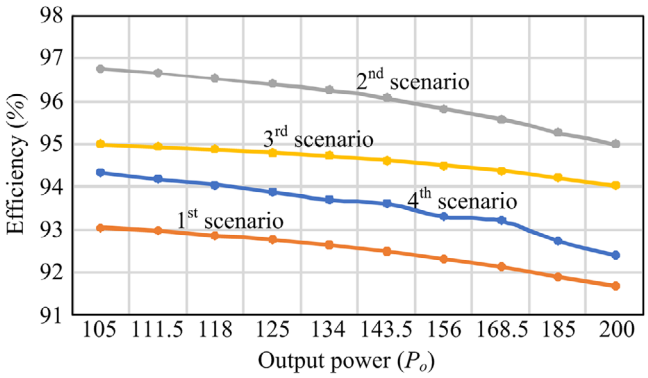

FIGURE 16 Efficiency curves in different scenarios and under different load conditions

10 | CONCLUSION

In this study, by conducting scientific research in continuation of previous works in the field of multi-port DC-DC converters, the result was to introduce and propose a new structure for non-isolated multi-port DC-DC converters. In the proposed structure, it is possible to charge and discharge the battery through the energy returned from the output. Also, the proposed structure has a high degree of flexibility, allowing the simultaneous and separate transfer of power from input sources as well as the possibility of charging the battery by another input. The functionality of the proposed converter in CCM was fully described and the static relationships governing it were extracted. The result is that the converter act as a boost converter in transferring power from the input to the output and as a buck converter in transferring power from the output load to the battery. Then, the minimum size of inductors and capacitor was determined to operate the circuit in CCM and to satisfy the allowable ripple of the output capacitor. The voltage stress of semiconductor elements was calculated. As a result, the proposed converters also have the advantage of lower semiconductor voltage stress, which has a significant effect on improving efficiency. Another important point is that the current of input sources is continuous. A small-signal model was obtained for the proposed structure. Based on the obtained small-signal dynamic model, a simple integral state feedback control system was designed. As a result of this control scheme, voltage and current control loops in different scenarios were considered. The proposed converter was also compared with other multi-port converters available in the references. Based on the results of comparisons, it was found that the proposed converter has good performance compared to other converters in terms of various factors, although it also has weaknesses. According to these comparisons, the proposed structure can be used in PV/Battery systems with significant positive points. The proposed structure was implemented and tested in the laboratory. According to the laboratory results, it was found that the performance of the proposed converter in different scenarios follows the results of theoretical analysis.

ACKNOWLEDGEMENT

The authors would like to express their gratitude to Iran National Science Foundation (INSF) for supporting the research in this article under Grant 98001298.

CONFLICT OF INTEREST

The authors have no conflict of interest to disclose.

ORCID

Naghi Rostami https://orcid.org/0000-0003-2018-7311
Seyed Hossein Hosseini https://orcid.org/0000-0002-3716-0126

REFERENCES

1. Pourfarzad, H., Saremi, M., Jalilzadeh, T.: An extended high-voltage-gain DC–DC converter with reduced voltage stress on switches/diodes. Electr. Eng. 102(4), 2435–2452 (2020)
2. Rajesh, R., Carolin Mabel, M.: A comprehensive review of photovoltaic systems. Renewable Sustainable Energy Rev. 51, 231–248 (2015)
3. Parida, B., Iniyan, S., Goic, R.: A review of solar photovoltaic technologies. Renewable Sustainable Energy Rev. 15(3), 1625–1636 (2011)
4. Hosenuzzaman, M., Rahim, N.A., Selvaraj, J., Hasanuzzaman, M., Malek, A.A., Nahar, A.: Global prospects, progress, policies, and environmental

impact of solar photovoltaic power generation. Renewable Sustainable Energy Rev. 41, 284–297 (2015)
5. Bhatnagar, P., Nema, R.K.: Maximum power point tracking control techniques: State-of-the-art in photovoltaic applications. Renewable Sustainable Energy Rev. 23, 224–241 (2013)
6. Mirhassani, S., Ong, H.C., Chong, W.T., Leong, K.Y.: Advances and challenges in grid tied photovoltaic systems. Renewable Sustainable Energy Rev. 49, 121–131 (2015)
7. Jalilzadeh, T., Rostami, N., Babaei, E., Hosseini, S.H.: Multiport DC–DC converter with step-up capability and reduced voltage stress on switches/diodes. IEEE Trans. Power Electron. 35(11), 11902–11915 (2020)
8. Jalilzadeh, T., Rostami, N., Babaei, E., Hosseini, S.H.: High voltage gain dual-input dual-output DC-DC converter with reduced voltage stress on semiconductors. Int. J. Circuit Theory Appl. 48(6), 934–952 (2020)
9. Jalilzadeh, T., Rostami, N., Babaei, E., Hosseini, S.H.: Bidirectional multiport dc–dc converter with low voltage stress on switches and diodes. IET Power Electron. 13(8), 1593–1604 (2020)
10. Rehman, Z., Al-Bahadly, I., Mukhopadhyay, S.: Multiinput DC–DC converters in renewable energy applications–an overview. Renewable Sustainable Energy Rev. 41, 521–539 (2015)
11. Khaligh, A., Cao, J., Lee, Y.: A multiple-input DC–DC converter topology. IEEE Trans. Power Electron. 24(3), 862–868 (2009)
12. Hintz, A., Prasanna, U.R., Rajashekara, K.: Novel modular multiple-input bidirectional DC–DC power converter (MIPC) for HEV/FCV application. IEEE Trans. Ind. Electron. 62(5), 3163–3172 (2015)
13. Nejabatkhah, F., Danyali, S., Hosseini, S.H., Sabahi, M., Niapour, S.M.: Modeling and control of a new three-input DC–DC boost converter for hybrid PV/FC/battery power system. IEEE Trans. Power Electron. 27(5), 2309–2324 (2012)
14. Ahrabi, R.R., Ardi, H., Elmi, M., Ajami, A.: A novel step-up multiinput DC–DC converter for hybrid electric vehicles application. IEEE Trans. Power Electron. 32(5), 3549–3561 (2017)
15. Akar, F., Tavlasoglu, Y., Ugur, E., Vural, B., Aksoy, I.: A bidirectional nonisolated multi-input DC–DC converter for hybrid energy storage systems in electric vehicles. IEEE Trans. Veh. Technol. 65(10), 7944–7955 (2016)
16. Deihimi, A., Mahmoodieh, M.E.S., Iravani, R.: A new multi-input step-up DC–DC converter for hybrid energy systems. Electr. Power Syst. Res. 149, 111–124 (2017)
17. Hou, S., Chen, J., Sun, T., Bi, X.: Multi-input step-up converters based on the switched-diode-capacitor voltage accumulator. IEEE Trans. Power Electron. 31(1), 381–393 (2016)
18. Amiri, E., Rahimzadehkhorasani, R., Adib, E., Khoshkbar Sadigh, A.: Multi-input high step-up DC-DC converter with independent control of voltage and power for hybrid renewable energy systems. IEEE Trans. Ind. Electron. 68, 12079–12087 (2021). https://doi.org/10.1109/TIE.2020.3047038
19. Rostami, S., Abbasi, V., Talebi, N., Kerekes, T.: Three-port DC–DC converter based on quadratic boost converter for stand-alone PV/battery systems. IET Power Electron. 13(10), 2106–2118 (2020)
20. KhademiAstaneh, P., Javidan, J., Valipour, K.., Akbarimajd, A.: A bidirectional high step-up multi-input DC-DC converter with soft switching. Int. Trans. Electr. Energy Syst. 29(1), e2699 (2019)
21. Faraji, R., Adib, E., Farzanehfard, H.: Soft-switched non-isolated high step-up multi-port DC-DC converter for hybrid energy system with minimum number of switches. Int. J. Electr. Power Energy Syst. 106, 511–519 (2019)
22. Askarian, I., Pahlevani, M., Knight, A.M.: Three-port bidirectional DC/DC converter for DC nanogrids. IEEE Trans. Power Electron. 36(7), 8000–8011 (2021)
23. Faraji, R., Ding, L., Esteki, M., Mazloum, N., Khajehoddin, S.A.: Soft-switched single inductor single stage multi-port bidirectional power converter for hybrid energy systems. IEEE Trans. Power Electron. 36, 11298–11315 (2021). https://doi.org/10.1109/TPEL.2021.3074378
24. Faraji, R., Ding, L., Rahimi, T., Kheshti, M., Islam, M.R.: Soft-switched three-port DC-DC converter with simple auxiliary circuit. IEEE Access 9, 66738–66750 (2021)
25. Zahedi Saadabad, N., Hosseini, S.H., Nasiri, A., Sabahi, M.: New soft-switched high gain three-port DC–DC converter with coupled inductors. IET Power Electron. 13(19), 4562–4571 (2020)
26. Pourjafar, S., Shayeghi, H., Sedaghat, F., SeyedShenava, S.J.: A dual-input DC-DC structure with high voltage gain suggested for hybrid energy systems. IET Power Electron. 14, 1792–1805 (2021). https://doi.org/10.1049/pel2.12149
27. Shayeghi, H., Pourjafar, S., Hashemzadeh, S.M.: A switching capacitor based multi-port bidirectional DC–DC converter. IET Power Electron. 14, 1622–1636 (2021). https://doi.org/10.1049/pel2.12137
28. Samadian, A., Hashemzadeh, S.M., Ghavipanjeh Marangalu, M., Maalandish, M., Hosseini, S.H.: A new dual-input high step-up DC–DC converter with reduced switches stress and low input current ripple. IET Power Electron. 14, 1669–1683 (2020). https://doi.org/10.1049/pel2.12143
29. Solero, L., Lidozzi, A., Pomilio, J.A.: Design of multiple-input power converter for hybrid vehicles. IEEE Trans. Power Electron. 20(5), 1007–1016 (2005)
30. Ogata, K.: Modern Control Engineering. Prentice-Hall, New Jersey (2002)
31. Kazimierczuk, M.K.: Pulse-width Modulated DC–DC Power Converters. John Wiley & Sons Ltd, Sussex (2008)

How to cite this article: Jalilzadeh, T., Rostami, N., Babaei, E., Hosseini, S.H.: Design, analysis and implementation of a new three-port DC-DC converter with bidirectional capability. IET Power Electron. 14, 2490–2506 (2021). https://doi.org/10.1049/pel2.12196